



# Triggered Seismicity in a Flooded Former Coal Mining Basin (Gardanne Area, France)

Pascal Dominique<sup>1</sup>  · Hideo Aochi<sup>1</sup> · Jacques Morel<sup>1</sup>

Received: 10 April 2021 / Accepted: 1 March 2022 / Published online: 4 April 2022  
© The Author(s) 2022

## Abstract

We studied the correlation between seismicity and the water table level in an abandoned coal mine (Bouches-du-Rhône, France), closed in 2003, where groundwater has been pumped out since 2010 to prevent underground flooding. Microseismicity was first felt by the population in 2010 and a strongly felt seismic swarm occurred in November 2012. The origin of the seismicity was therefore questioned, in relation to both the potential instability of old, shallow galleries that might generate damage at the surface and a local seismic hazard assessment. A temporary dense seismic network in the area allowed us to analyse the spatial distribution of the seismicity in detail. Most of the seismicity was clearly located under the mine workings, highlighting that an existing fault system crossing the mining operation was being hydraulically activated, in accordance with the known tectonic extension regime. Our analysis clearly shows a spatiotemporal relationship between seismic migration and the level of the mine aquifer between 2013 and 2017. Thus, seismicity will persist with oscillations of the mining aquifer, depending on the pumping capacities and effective rainfall. Continuous hydraulic and seismic monitoring is necessary to better understand these phenomena and assess the associated risks.

**Keywords** Post-mining seismicity · Mine aquifer · Seismic migration · Rock burst

## Introduction

The Gardanne coalfield is located in Provence, southern France, between the towns of Marseille and Aix-en-Provence. Coal was exploited from the beginning of the seventeenth century until 2003. The first exploitation was performed along shallow seams directly from the surface. Then, room-and-pillar techniques were used down to a depth of 700 m, while the deepest exploitation, down to a depth of 1300 m, used longwall mining. Approximately 130 Mt of coal was extracted from the Gardanne coal mine.

The long historical experience of the mining industry has shown that underground works exploited with room-and-pillar techniques can lead to mechanical instabilities, especially when groundwater fluctuations occur. With time, pillars left in place deteriorate, and the process that can be accelerated

in the presence of water, sometimes leading to the failure of one or several pillars, with potential damage to the surface (Goldbach 2010; Senfaute et al. 2008).

As coal exploitation ceased in 2003, the halt of pumping operations led to progressive flooding of the underground mine workings until the mine groundwater level quasi-stabilized in 2010, though it still fluctuates. To survey the risk of mechanical instabilities associated with room-and-pillar sectors below inhabited areas, a permanent microseismic network was installed at the end of 2007, which has since been monitored by Ineris (French National Institute for Industrial Environment and Risks) on behalf of BRGM (French Geological Survey). This network consists of five microseismic stations located in the immediate vicinity (a few hundred meters) of these room-and-pillar sectors and seismic sensors positioned in boreholes at different depths. This network detects any microseismic event within a radius of 400 m around the stations and monitors potential microseismic activity induced by rock fracturing associated with underground mine workings deterioration. The intent is to identify any risks with potential consequences to the surface, and thus protect the population.

✉ Pascal Dominique  
p.dominique@brgm.fr

<sup>1</sup> Risks and Prevention Department, BRGM, Bureau de Recherches Géologiques et Minières, 3 Ave Claude-Guillemain, BP 36009, 45060 Orléans Cedex 2, 45060 Orléans, France

Since 2010 and especially November 2012, several seismic swarms lasting a few days have occurred outside these ground instability surveillance zones. The seismic vibrations regularly felt by the population in the Fuveau-Greasque (FG) area have led the administration and local authorities to request the deployment of temporary complementary surface seismic network to determine their origin, including the possibility that pre-existing faults were being reactivated.

Therefore, the first purpose of this study was to verify whether these seismic ground motions are the result of the collapse of old mining galleries (roof collapse) or related to ruptures along pre-existing tectonic faults. In both cases, the role of water and fluctuations of the mine aquifer level are important. The second purpose was to correlate the spatiotemporal evolution of the seismicity with the water level in the mine workings.

## Geological and Hydrogeological Settings

## Geological Setting

Western Provence is part of the Pyrenean-Provençal domain in southern France (Fig. 1). The tectonic formation of western Provence occurred at the end of the Eocene. It has four structural units: the Bandol, Beausset, Arc, and Durance units (Rouire 1979).

The Arc unit lies between the North Provençal and South Provençal overlaps. In the west, it disappears beneath the Rhodanian Quaternary to the west of the Salon-Cavaillon fault (SCF). In the east, it ends at the level of the Trias of Barjols, beyond which the tectonic style and the Mesozoic characteristics are different. The E-W faults of La Nerthe, L'Etoile, Sainte-Baume, and Allauch belong to the Arc unit. Therefore, the Arc unit extends to the south under the southern Provençal overlaps of Etoile, Nerthe, and Sainte-Baume, while to the north, the overlaps of Fare and Aix-Eguilles cover the unit.

Locally, the basin is limited to the south by the overlapping east–west running Diote fault (DF), which extends

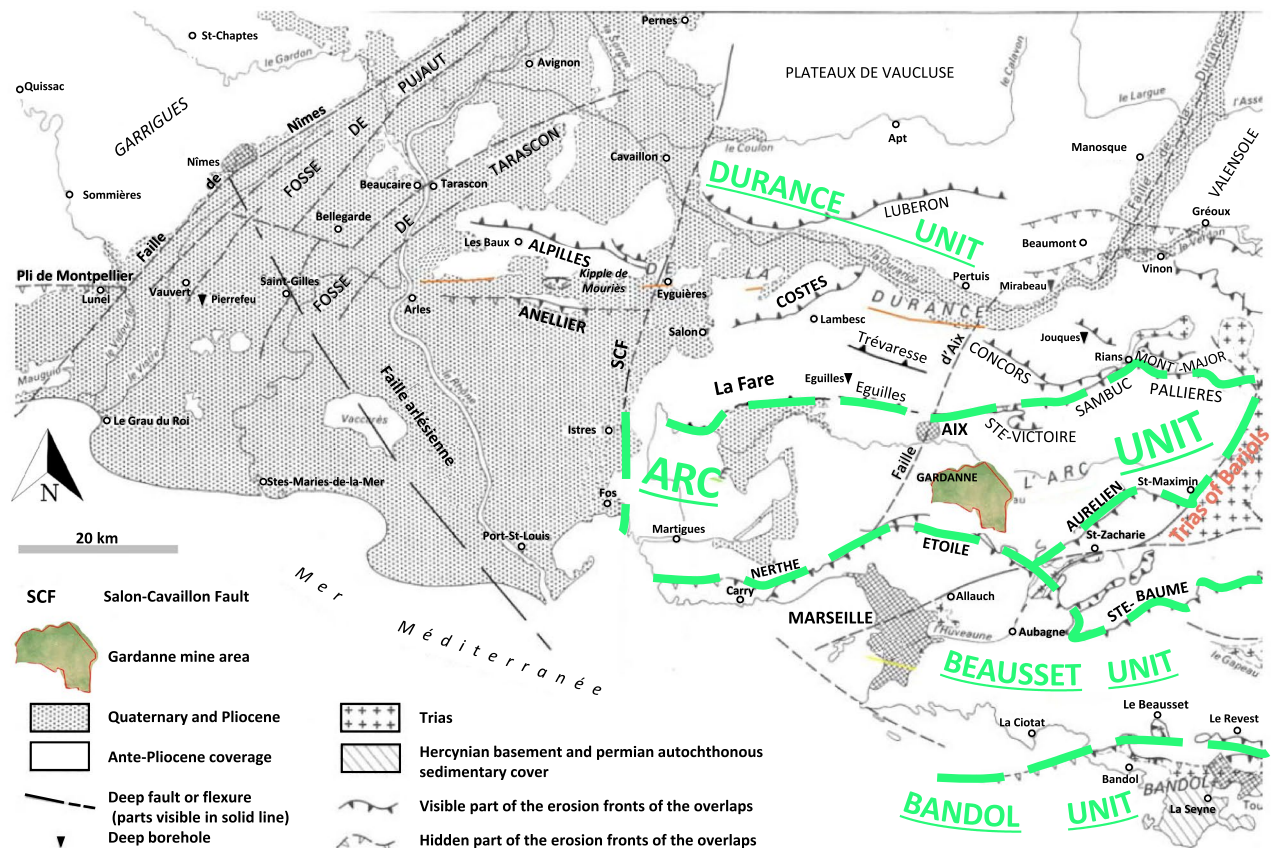


**Fig. 1** Geological units in the Pyrenean-Provençal domain (after Rouire 1979, modified)

further to the Jean-Louis fault (JLF) in the east. The sub-meridian Meyreuil fault (MF) is an extension of the Durance fault from the north to south. It crosses the Gardanne Basin and affects both the indigenous lands of the Arc Basin and the overlapping Diote fault (Fig. 2).

## Stress State

Based on seismicity data and focal mechanisms, large-scale studies near the outer boundaries of the western Alpine Belt highlight the strain/stress state of this western Provence area (Baroux et al. 2001; Delacou et al. 2004), suggesting an extensional stress (normal faulting) regime represented by a NNW-SSE trend for the horizontal principal stress axis,  $\sigma_1$ . Geodetic data confirm this trend (Calais et al. 2002), even if the strain rate is very low (less than 0.01  $\mu\text{strain/yr}$ ), as well as the horizontal and vertical GPS velocities (less than 1 mm/yr) (Devoti et al. 2017).

At the Gardanne mine site, Gaviglio (1987) and Gaviglio et al. (1996) obtained stresses at a very local scale

from in situ measurements (flat jack method or hydraulic fracturing). They showed that two zones of stress state can be distinguished (Fig. 2): one isotropic northern extension zone and another anisotropic southern compression sector. The northern zone presents mainly as an extension to N45°E, particularly in the inflection zone (with a vertical stress very close to the N135°E maximal horizontal stress), whereas the southern zone briefly corresponds with an anisotropic compression of E-W to NE-SW. A sub-meridian extensional stress in the north-eastern part of the area has been mentioned (Chalumeau 2000; Didier et al. 2003).

## Hydrological and Hydrogeological Contexts

The above stress state studies were confirmed in Chalumeau's (2000) thesis, using the geomorphology method. Moreover, the author described this disconnection and its separate hydrogeological behaviour (Fig. 2). Indeed, due to the very strong inflow of water from the surrounding massifs

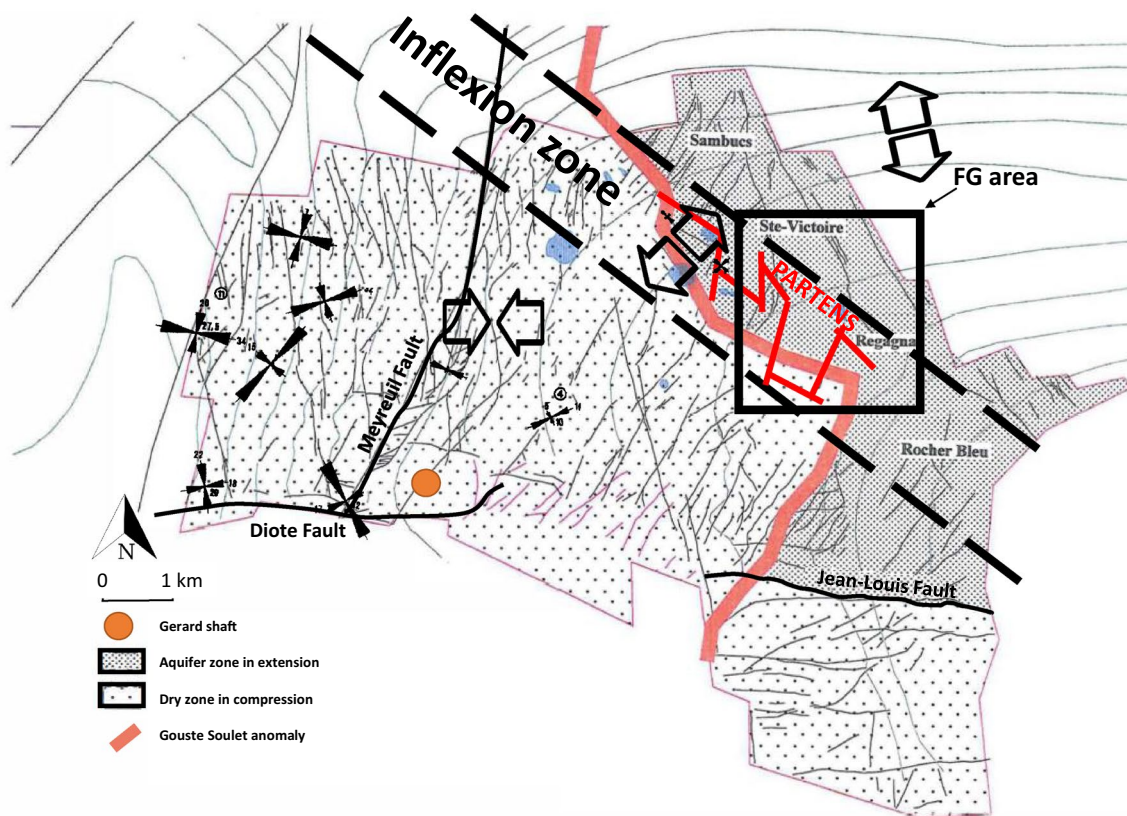


**Fig. 2** Gardanne mine area with stress state (after Gaviglio 1987; Gaviglio et al. 1996, modified) separating the southwestern dry zone in compression and the northeastern aquifer zone in extension (after Chalumeau 2000, modified). Arrows represent magnitudes and orientations of the principal stresses determined for each site (Gaviglio et al. 2016). Large hollow arrows give the stress state (extension or

compression) and its mean azimuth (Gaviglio 1987; Chalumeau 2000; Didier et al. 2003). Locations of "Partens" are represented by red lines (after Moulin 2010, modified). Main faults (bold black lines): Diote Fault, Meyreuil Fault and Jean-Louis Fault. Pumping Gerard shaft (orange dot). The bold black square corresponds to the FG area in the present study

(Sainte-Victoire and Regagnas), the development of underground operations was particularly difficult in the northeastern part of the Gardanne mine area (Fuveau-Greasque (FG) area). Thus, many drainage galleries were excavated to limit the costs of pumping at the level of the shafts. Likewise, even the construction of several dams to block the galleries could not prevent the abandonment of some mining districts, such as the Rocher Bleu district. These significant inflows of water are linked to several factors:

- The presence of a vast natural impluvium corresponding to the Arc Basin collecting all rainwater from the limestone massifs of Sainte-Victoire to the north and northeast, from the Regagnas (southeast) and from l'Etoile (south). Dheilly and Brigati (2015) credited the origin of the main water inflows to the Gardanne mine to surface infiltration from the Fuvelian and Begudian outcrops and deep-water inflows (mainly Jurassic) from the sources of the Sainte Victoire at -220 m ASL (above sea level), Source 90 at -50 m ASL, and Massif de l'Etoile.
- The connection of different aquifers from the most superficial to the deepest (Begudian (Upper Cretaceous; 66–772 My), Fuvelian (Upper Cretaceous; 72–84 My) and especially Jurassic (145–200 My)) is favoured by the existence of open fractures (partens) and karstified zones with a strong infiltration of water at depth. The local extensional stress favours these aquifer interconnections (Chalumeau 2000).

The main level of mining, called the Grande Mine, is  $\approx$  2 m thick. Outcropping over the Greasque sector, the Grande Mine layer gradually deepens towards the northwest, reaching a depth of  $\approx$  330 m below the FG area. This deepening continues to the west until it reaches 1300 m west of Gardanne. The residual voids of the Grande Mine layer correspond to a privileged drain of all these mining aquifers—mainly the Jurassic Aquifer—facilitating the circulation of water (volume, flow, transfer time) from East to West.

In contrast, compressed zones of lower permeability are found in the southwestern sector close to certain faults that sometimes act as barriers, such as the Jean-Louis fault to the south of the Rocher Bleu (Chalumeau 2000). Likewise, the clayey Valdonian (upper Cretaceous; 72–84 My) and marl limestone Neocomian (lower Cretaceous; 129–145 My) impede the circulation of water between aquifers (Gonzalez 1990).

## Management of Mine Water in the Gardanne Coal Mine

After mine closure, pumping of the Jurassic aquifer at a flow rate of 1500 to 2000 m<sup>3</sup>/h at the Arc shaft was shut down on May 3, 2003. This led to the natural rise of the

groundwater level, with a progressive flooding of the mine workings starting from the deeper parts on the western side and progressing towards the east. To avoid overflow of mineralized water rich in iron and sulfate (due to sulfides in the oxidized lignite) contaminating the port of Marseille and flooding hazards at the surface, water flow has been again controlled by pumps set in a former Gerard mine shaft (see Fig. 2). As pumping resumed (August 4, 2010), the water level in the mine reservoir rose from -1100 m ASL to -14 m ASL. Between 15 and 45 Mm<sup>3</sup> of mine voids were saturated. Hydrological models (Dheilly and Brigati 2015) integrating water level pumping capacities and effective rainfall show that a constant mine aquifer (as described above) of 800 m<sup>3</sup>/h supplies the mine reservoir. An additional volume of 200 to 1000 m<sup>3</sup>/h depends on the annual effective rainfall. All these volumes are pumped at the Gerard shaft in Gardanne (+18 m ASL) and discharged by a 14 km pipeline outside the Marseille harbour, at a depth of 30 m, in the Mediterranean Sea. Thanks to the pumping system, the mine groundwater is stabilized between -30 m ASL and +10 m ASL,  $\approx$  250 to 350 m below the ground surface in the FG area. To prevent pollution and flooding, the mine water level must be maintained between +18 m ASL (flooding level in the Galerie de la Mer) and -35 m ASL (pump level at -40 m ASL).

The mine water level is monitored remotely. A high-flow pumping test (3000 m<sup>3</sup>/h) was performed between mid-July and the end of September 2014 in the Arc shaft, located 12 km east of the Gerard shaft. The water in the Jurassic aquifer comes from rainfall at the heights of the Sainte-Victoire and Regagnas massifs. This pumping and the slope rupture of the water level recorded in the Gerard shaft established the connectivity of the aquifer between the two shafts with a delay of 1.5–2 days (Dewandel et al. 2017), and the strong influence of inflows from the Jurassic aquifer in the Arc Basin (Dheilly and Brigati 2015).

## Seismic Context

### Seismicity Near the Gardanne Coal Mine

Over the past five centuries, several earthquakes have strongly shaken the Provence region. Historical data show a relatively sparse epicentral distribution of earthquakes (Sis-France 2016; Jomard et al. 2021). Some earthquakes highlight regional faults, such as the Moyenne Durance, Nîmes, Salon-Cavaillon, or Trevaresse Faults (Figs. 1, 3a).

The Lambesc earthquake on June 11, 1909 (Baroux et al. 2003) was the most destructive of the twentieth century in France. With an intensity of VIII-IX and a moment magnitude of Mw5.7 (Baroux et al. 2003; Manchuel et al. 2017), it caused 46 deaths, 250 injuries, and the partial destruction

of some villages near the epicentre (Rognes, Saint-Cannat, and Lambesc) and part of the town of Salon-de-Provence (SisFrance 2016). Other notable tremors occurred in the Bouches-du-Rhône (Fig. 3) on May 28, 1985, (intensity V and Mw2.6), in Vernègues on December 23, 1934, in

Salon-de-Provence (IV-V and Mw3.3) on December 12, 1846, in Gemenos (VI and Mw3.9), on March 25, 1783, and in Mallemort (V and Mw3.2) and Arles between 1725 and 1734. The oldest recorded earthquake dates from May 26, 1397 (V-VI and Mw3.5) in Arles. We also note the events

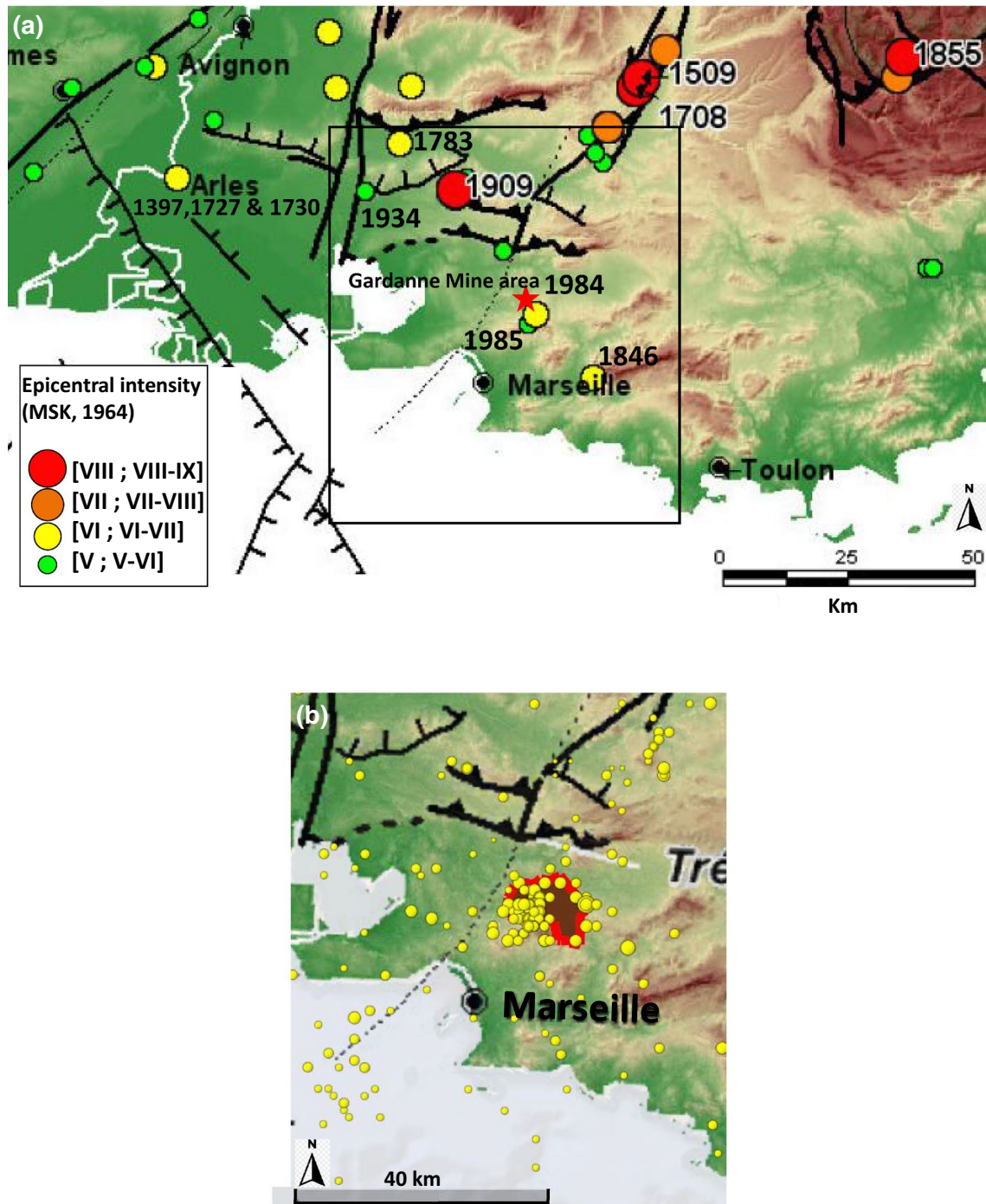


**Fig. 3** Seismicity around the Gardanne Mine. **a** Historical seismicity from the macroseismic database (SisFrance 2016). The black rectangle is the zoomed area shown on the right. **b** Instrumental seismic-

ity from the SI-Hex catalogue (1962–2009, Cara et al. 2015). The red star (a) and red zone outline (b) are the Gardanne coalmine areas (modified from Terrier et al. 2008)

of the Middle Durance (1509, 1708, 1812, 1863, and 1913), some of which reached epicentral intensity VIII.

Specifically, in the Gardanne coal mine area, the February 19, 1984 (VI and Mw3.6) Mimet earthquake has been studied regarding its origin: artificial or natural (Haessler et al. 1985). Based on a spectral analysis of aftershocks, the authors showed that the nature of the signal was very close to that of a tectonic earthquake. Hence, regardless of the contradiction between the focal mechanism, the regional stress state, and the hypocentral location that favours an event associated with mine exploitation, they concluded that this February 19, 1984 shock was not caused by a mine collapse, but was likely due to a local modification of the regional stress field induced by mine exploitation.

Great effort has been made by the SI-Hex Working Group (Cara et al. 2015) to discriminate between natural and artificial earthquakes. Nevertheless, Fig. 3b shows a cluster of seismic events centred on the Gardanne coal mine. It is possible that this seismic activity is linked to natural activity or to artificial activity during the exploitation of the coal mine. Based on the very well-constrained location for recent seismic events and on the work performed on the slight amelioration over time of the RMS precision of the location between 1962 and 2009 in this Provence area (Cara et al. 2015), a location error of approximately 10 km is considered, especially for lower magnitudes, i.e., less than Mw2.5. Then, if we take into account a radius of almost 10 km around the Gardanne coal mine, and even less, there is a clear cluster of seismicity in this area, particularly during exploitation until February 2003. This seismicity seems to have continued in recent years but at a lower level. These observations obtained from French national networks (gathered within the research infrastructure of the French seismological and geodetic network RESIF-EPOS—[www.resif.fr](http://www.resif.fr)) provide a global view in recent decades. After the closure of the coal mine in February 2003, a local seismic network at the scale of the Gardanne mining basin with the specific objectives detailed above has been operated by Ineris since the end of 2007. Following the occurrence of events strongly felt by the population, seismic monitoring has been reinforced by the BRGM (since mid-2013). Local

networks reveal local-scale seismic activity in the former coal mine area.

As stated above, this paper focuses on the recent seismic activity obtained by the deployment of a temporary seismic network during the 2013–2017 period in a specific area of the former Gardanne coal mine (FG area).

## Fuveau-Greasque Seismic Activity

The inhabitants of the Le Jas de Bassas and Galoubet districts (commune of Fuveau) first felt “significant vibrations” during the month of June 2010. These observations coincided with the seismic activity recorded by the permanent Ineris network (Dünner 2011). No recorded seismic events or evidence of vibrations was known in this sector before 2010, following the flooding of the mine workings.

On November 1, 2012, at 3:58 am at local time (2h58 UT), a seismic event followed by a seismic swarm was widely felt by the population of the communes of Fuveau (west) and Greasque (north) for about three days. The lack of automatic reports by the French Alternative Atomic Energies and Atomic Energy Commission (CEA) and SISMALP Observatory and the local testimonies of populations indicate a low energy event (magnitude probably less than 2.5) and a superficial origin (less than 5 km). This seismic event was manually determined by different networks/organizations, such as Ineris, CEA, OCA (Côte d’Azur Observatory, Nice) and RéNaSS (National Network of Seismic Surveillance, Strasbourg) (Table 1). As mentioned above, epicentral determination uncertainties for national seismic observatories (CEA, RéNaSS) can reach 10 and even 30 km.

## Methods

### Local Temporary Seismic Network of the Fuveau-Greasque Area

Following this seismic swarm, the State decided to strengthen the microseismic monitoring system in the eastern Provence coal basin by supplementing the system set up

**Table 1** Characteristics of the seismic event on November 1, 2012. Md (duration magnitude), MLv and MI (local magnitude), and Mw (moment magnitude)

| Organization | Origin Time (TU) | Latitude                 | Longitude               | Magnitude                      | Depth (km) | Suspected type |
|--------------|------------------|--------------------------|-------------------------|--------------------------------|------------|----------------|
| Ineris       | 02h58 31         | 43°26.520'N              | 5°31.678'E              | Md 2.9                         | 0.55       | Mine collapse  |
| OCA          | 02h58 30         | 43°29.100'N<br>± 42.5 km | 5°36.900'E<br>± 19.4 km | MLv $2.57 \pm 0.38$<br>Mw 3.15 | -          | -              |
| CEA          | 02h58 33         | 43°24.852'N<br>± 3.1 km  | 5°32.826'E<br>± 1.4 km  | MI $2.2 \pm 0.38$<br>Md 2.2    | 2          | Induced event  |
| RéNaSS       | 02h58 28         | 43°09.900'N<br>± 10 km   | 5°28.200'E<br>± 5 km    | MLv 2.2                        | 0 (fixed)  | Quarry blast   |

in 2013. A temporary network of four stations, growing to five in 2015 and then nine in 2018, was installed by BRGM in the area (Fig. 4). Three-component accelerometers are located on the ground in private homes. Although the background noise level is not optimal, this network was deployed

quickly at a low cost and has allowed us to follow the continued seismic activity, including the seismic swarms that occurred in 2014, the end of 2016, and in 2017. To achieve good sampling for signal processing, the acquisition was set to 1000 Hz. The triaxial broadband accelerometric sensors

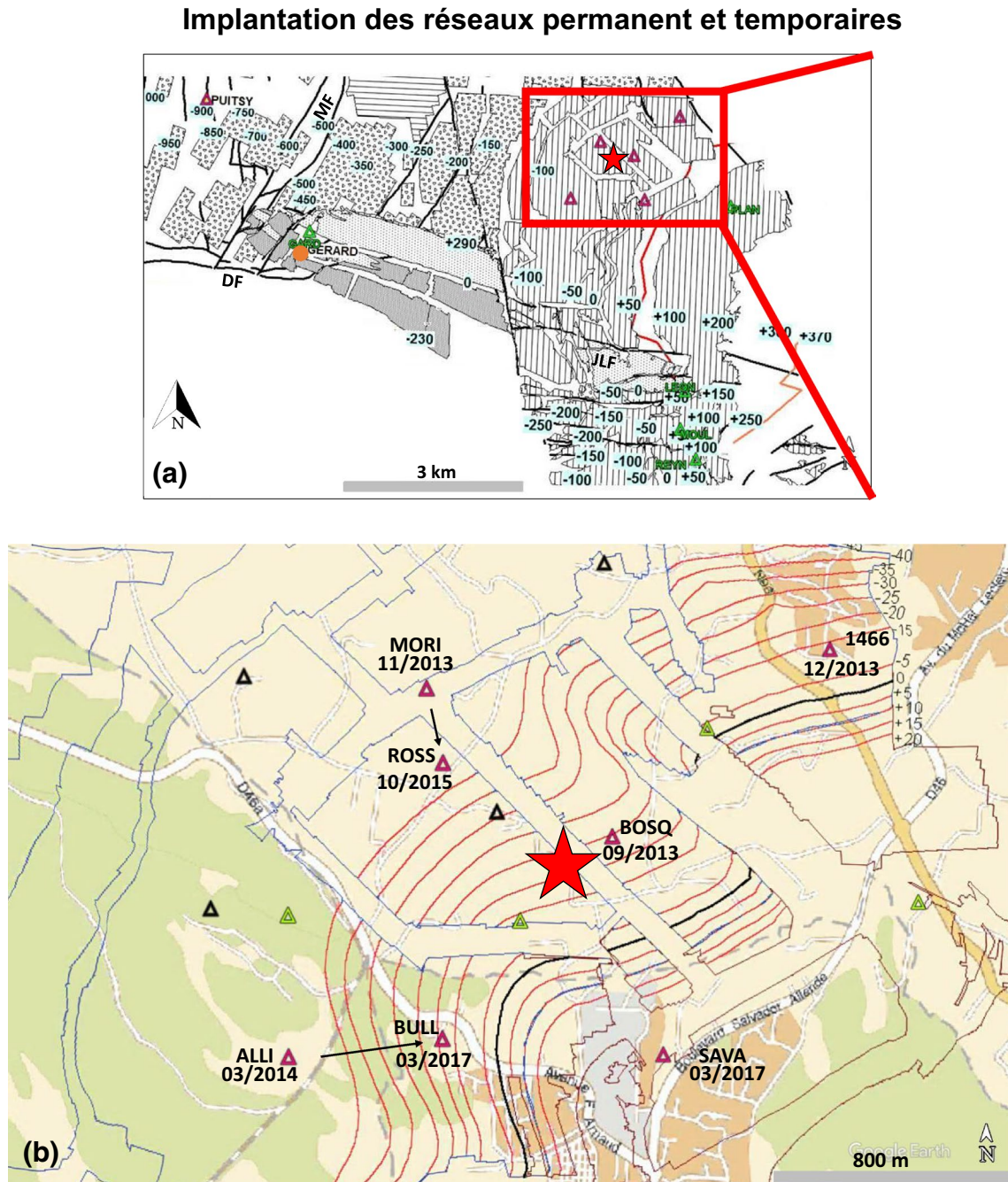


**Fig. 4** Evolution of the temporary seismic BRGM network. **a** Five temporary BRGM stations (purple triangles) are superimposed on a map of the Gardanne coal basin. Ineris permanent network (green triangles). Main faults (bold black lines): *DF* Diote Fault, *MF* Meyreuil Fault, and *JLF* Jean-Louis Fault). Location of the seismic swarm in 2012 (red star). The pumping Gerard shaft (orange dot) and type of mine workings: room and pillars (vertical lines), long walls (dots), and backfilling (horizontal lines and grey area). The numbers are the ASL of the mine workings. **b** Zoom of the FG area where the temporary BRGM network is installed (purple triangles) with the date of installation. Some stations have been moved (black arrows). Other stations (green triangles (Ineris) and black triangles (BRGM)) were installed later in 2018 and 2019. The lines represent the ASL of the mine workings with the corresponding value in the top right side

and backfilling (horizontal lines and grey area). The numbers are the ASL of the mine workings. **b** Zoom of the FG area where the temporary BRGM network is installed (purple triangles) with the date of installation. Some stations have been moved (black arrows). Other stations (green triangles (Ineris) and black triangles (BRGM)) were installed later in 2018 and 2019. The lines represent the ASL of the mine workings with the corresponding value in the top right side

thus allow the recording of regional seismicity as well as small local events without risk of signal saturation in the case of strong motion. This complementary seismic network acquires data continuously or at a triggering threshold. Figure 4a shows the deepening of mine workings from east to west. In the FG area (Fig. 4b), the deepening angle is very low, with a dip of 3° to 7° towards the northwest.

## Data Processing

We use an adapted version of the HYPO71 location program (Lee and Lahr 1975) to locate seismicity. The velocity model is based on borehole log profiles and on knowledge of the geology. A velocity model over the Gardanne area provided values for compressional P-wave velocities ( $V_p$ ) and shear S-wave velocity ( $V_s$ ) for different geological layers (Bertil et al. 1987). We have refined this model, including the ratio of compressional wave velocity to shear wave velocity,  $V_p/V_s$  (Table 2) by minimizing the residues on the arrival times of the waves and the root mean square error (RMS) obtained at the locations. Some tests on quarry shots allowed us to check the velocity model and  $V_p/V_s$  ratio, and to validate the location results. The significant variations in water saturation of the locally saturated environment at  $\approx 0$  m ASL depth and oscillations of several meters to tens of meters could also affect this ratio. The RMS on all residuals of the travel times to the stations obtained by location by HYPO71 is less than 0.01 s for all events, which indicates a correct quality of the locations. We determined that the location uncertainty of local seismic events is almost 50–100 m inside the temporary network and 100–200 m outside.

Another point is the local response of the sites, which is a key element of any seismological and seismic hazard analysis. The use of background noise recordings generally allows the experimental determination of lithological site effects that may significantly modify the soil response (Nakamura 1989). This is also ideally suited to regions with moderate seismic activity, where there are few records of ground motion, and to urban or industrial contexts, where the noise level is potentially high (Bour et al. 1998). The characterization of the soil responses permits us to evaluate any overestimation of the signal that could have an impact on the calculation of the magnitude.

**Table 2** Seismic velocity model adopted for this study with  $V_p/V_s = 1.9$

| Depth (km) | $V_p$ (km/s) |
|------------|--------------|
| 0–1        | 3.85         |
| 1–4        | 5.0          |
| 4–15       | 5.7          |
| 15–25      | 6.7          |
| > 25       | 8.0          |

We checked the noise environment of seismic stations that record the events. For all seismic stations, the soil responses were flat, and the horizontal to vertical spectral ratio H/V was less than 2, i.e., there was no observation of apparent site effect. In contrast, the systematic calculation of local magnitude based on amplitude and distance shows that the farthest northeastern station, “1466”, could underestimate the amplitude of the seismic signal regardless of the location of the event inside the network. This could be due to the poor condition of the sensor installation, which is not firmly anchored to a hard floor.

Finally, a seismic catalogue based on manual pickings of P and S arrivals of 2688 events was established between mid-2013 and December 2017. Then, for some large magnitude events of each sequence, we calculated the focal mechanism using full waveform inversion in a limited frequency band (Aochi and Burnol 2018). The elastic response to a unit double-couple force (Green's functions) are calculated using the same 1D model in Table 2. We fixed the epicentre position and varied the focal depth to minimize the misfit, which was calculated for the L-2 norm (least squares). We chose to directly invert the focal mechanism of the double-couple seismic moment (three parameters: strike, dip and rake) rather than the six independent moment tensors. Additionally, the moment magnitude (Mw) and origin time ( $t_0$ ) are unknown. The parameters were searched using a genetic algorithm (Goldberg 1989) that has previously been adopted in similar inversions (Ulrich and Aochi 2015; Aochi and Burnol 2018).

## Results

### Seismicity and Ground Motion Record

The BRGM temporary network successfully revealed the unexpected number of local seismic events in the FG area (Fig. 5, Supplemental Fig. S-1). We could detect three times more events than those detected using the Ineris permanent network. Correlatively, the threshold of magnitude detection was improved from 0 down to –0.5 or even less.

Nearly 2688 seismic events were detected and located between October 2013 and December 2017, with some swarms generating up to 250 events per day. Typically, these swarms for the most part were felt by the population and lasted a few days: November 1 to 3, 2012; December 1 to 4, 2014; December 8, 2016; January 21, 2017; January 31 to February 2, 2017; February 6 to 7, 2017; February 17 to 18, 2017; March 9 to 10, 2017; August 22 to 24, 2017; and September 8, 2017. At the end of 2021, only one swarm has occurred on June 12 and 13, 2021 since 2017. The main swarms occurred during the winter season, except for that

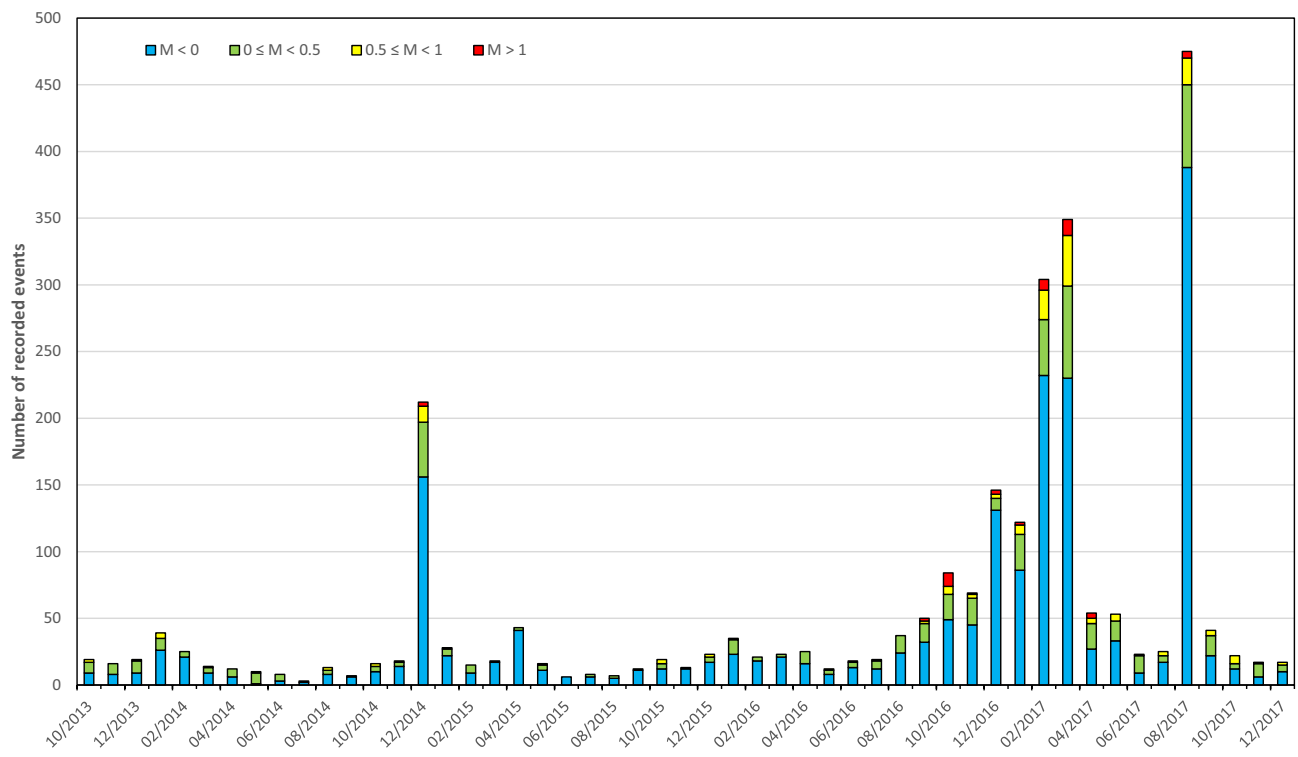


**Fig. 5** Histogram of the FG area seismicity showing the number of seismic events per month from October 2013 to December 2017. We can distinguish the seismic swarms of December 2014 and August

2017, as well as the seismic activity that increased from mid-2016 until the beginning of 2017

in August 2017. The main characteristics of this seismicity are discussed later.

Figure S-2 in the supplemental information file shows a plot of the peak ground acceleration (PGA), defined as the maximum values of the vector sum of the three component acceleration time histories, with respect to hypocentral distance. Based on the relationship between PGA and intensity (Worden et al. 2012), almost 15% of the recorded PGA values were susceptible to be felt by the population, and the highest PGA values reached the threshold of very slight damage to buildings from mid-2013 to late 2017. We also observed that the hypocentral distances of the recorded events were mostly between 0.4 km and 2 km. As most focal depths were from 400 to 800 m, the epicentral distance was of the same order as, or even less than the depth.

### Focal Mechanism and Implications

Table 3 and Fig. 6 summarize the focal mechanisms we obtained. We chose a different bandpass filter at  $\approx 1$  Hz to clearly extract the pulse and varied the focal depth every 100 m with respect to the location catalogue. We do not always use the closest station for each event to avoid any uncertainty of the seismic event location. Globally, we could fit the waveforms well. For seismic events of magnitudes

less than 1.3, the signals were not strong in this frequency range, which made it difficult to extract the main phase of the signals from the background noise level. We adopted the focal depth that produced the minimum misfit, and the result was consistent with the catalogue. All the analysed seismic events were found to be deeper than the mining gallery, indicating reactivation of the natural fault system.

All obtained mechanisms show normal faulting, mostly NW–SE strikes. The strike trend inferred from the fault mechanism should be discussed statistically, as the quality of the result varies one after another due to the number and coverage of the stations, the S/N ratio and a complex source mechanism. Under these limitations, the solution may not always be unique. For the example presented in Fig. 6, the waveform fitting is sufficiently good for the largest event on January 31, 2017. Although the best solution indicates a fault strike in the NW–SE direction, the second preferable solution still has a strike of N210°E (NNE–SSW). We cannot simply average them, as each solution might have a local minimum. However, among the different global searches of the parameters indicating the same strike direction, the variation remained small for this event (for example, strike and dip less than a few degrees and rake less than 10°). On the other hand, the records of the second largest event on December 1, 2014, showed two bursts of energy in the

**Table 3** Parameters of the obtained focal mechanism analysis for large magnitude events. Mw: moment magnitude;  $M_{\text{BRGM}}$ : local magnitude; and  $M_{\text{Ineris}}$ : duration magnitude. Although this paper focuses

on seismicity from mid-2013 to December 2017, we also show the focal mechanisms of recent seismic events in 2018 and 2019 for a better understanding

| Date       | Mw   | $M_{\text{BRGM}}$<br>$M_{\text{Ineris}}$ | Strike<br>(°) | Dip<br>(°) | Rake<br>(°) | Depth (m) | Filtered band (Hz) | Used stations | Available stations |
|------------|------|--|---------------|------------|-------------|-----------|--------------------|---------------|--------------------|
| 2014/12/01 | 1.76 | 1.3<br>2.3                               | 216           | 69         | -90         | 700       | 0.75–1.5           | 3             | 4                  |
| 2016/10/21 | 1.40 | 1.4<br>2.4                               | 322           | 28         | -100        | 300       | 1.5–3              | 3             | 5                  |
| 2017/01/31 | 1.9  | 1.7<br>2.2                               | 309           | 51         | -96         | 670       | 1–2                | 5             | 5                  |
| 2018/08/29 | 1.25 | 1.0<br>2.1                               | 283           | 38         | -106        | 520       | 1–2                | 4             | 5                  |
| 2019/01/16 | 1.34 | 1.2<br>1.9                               | 291           | 48         | -100        | 470       | 1–2                | 9             | 9                  |
| 2019/04/19 | 1.41 | 1.3<br>2.3                               | 262           | 47         | -75         | 470       | 1–2                | 8             | 9                  |

seismograms, indicating two events. Thus, the obtained mechanism should be regarded as a mean feature of the total process. From Table 3, the NW–SE striking mechanism (four among the six events analysed here) had an average of N301°E (N59°W), indicating the representative tectonic system shown in Fig. 2. The tectonic interpretation also indicates different directions of distensive stress and open

structures (partens) in the surroundings; therefore, the diversity of the focal mechanism may have mechanical causality (Fig. 2).

## Seismicity and Hydrological Considerations

As described above, the mine water level often fluctuates. These variations are due to the pumping capacity mainly at

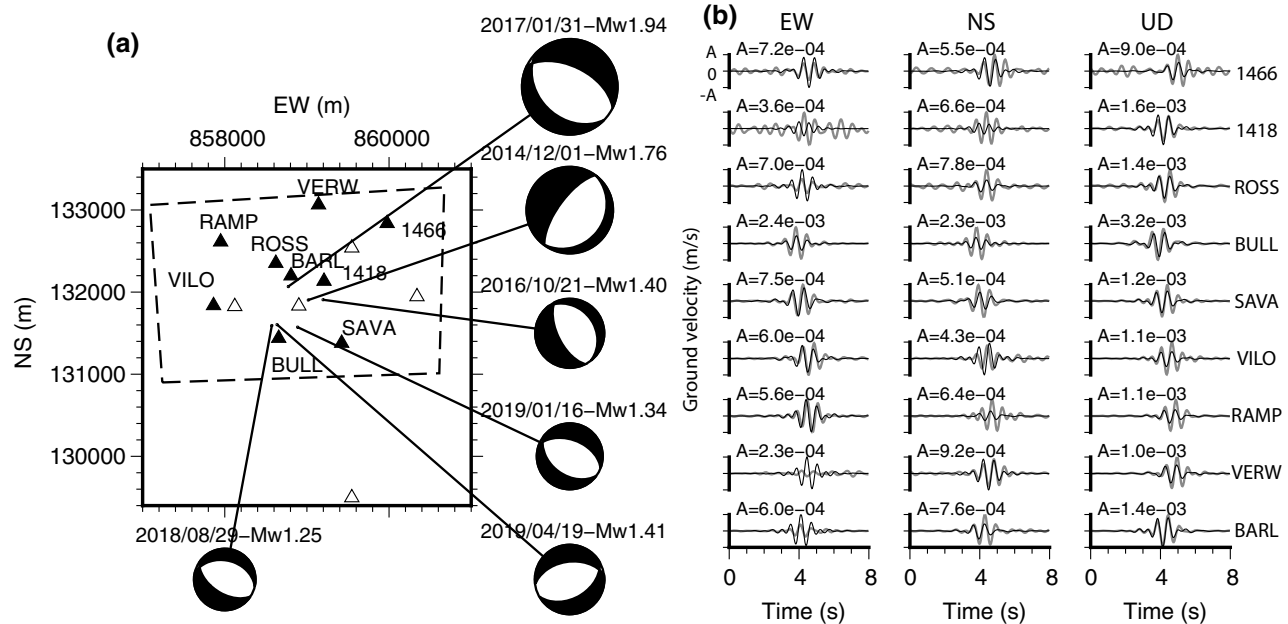


**Fig. 6** **a** Focal mechanisms for the seismic events listed in Table 3. The solid and open triangles represent the BRGM stations and the other network, respectively. BRGM stations are only used for the focal mechanism analyses. The framework by the broken lines indicates the FG area shown in Fig. 4b. **b** The fitting of seismograms for

the 2019/01/16 Mw 1.34 event. The velocity waveforms are filtered between 1–2 Hz for both the synthetics (black lines) and the observations (grey lines). The amplitude is normalized for each panel with a constant A

the Gerard shaft and effective rainfall. This term “effective” is used because it alone contributes to the reconstitution of aquifers and depends regionally on the type of soil. The data are recorded in Aix-en-Provence.

In 2010 (February, May, and especially June), some seismic activity was recorded on the permanent Ineris seismic network in the FG area, although no events had been detected since its installation on November 1, 2007 (Dünner 2011). Moreover, no event had been felt since the mine closure in 2003. As shown in Fig. 7, this time coincided with the reaching of the  $-30$  m ASL of the mine water table at the pumping Gerard shaft (Fig. 4). We can also distinguish three periods of mine aquifer evolution, depending on pumping capacity and rainfall after 2010 (green curve in Fig. 7):

- In the first period, from mid-2010 to mid-2016, the seasonal fluctuation in the level of the mine aquifer was on the order of 20 m (approximately between  $-10$  m ASL and  $+10$  m ASL).
- The second period, from mid-2016 to the end of 2017, when four pumps were replaced at the same time as a

very dry period, which produced a decrease in the water level of  $\approx 20$  m, reaching the water levels in early 2010 (from  $-10$  m ASL to  $-30$  m ASL) by the end of 2016.

- Since the end of 2016, these levels have stabilized, with smaller fluctuations of about  $-30$  m ASL.

We focus now on these three periods, with an emphasis on the locally instrumented period from the end of 2013 to the end of 2017.

#### First Period (mid-2010 to mid-2016)

In the first period, a previous study (Dominique 2016) distinguished two types of seismicity between mid-2013 and the end of 2015 triggered by oscillations of the water table:

- One, rather sparse type, on a kilometric or plurikilometric scale, with migration for several months, which followed the level of the mine water table. This microseismicity, often not felt by the population, was of low magnitude and can be considered microseismic background noise

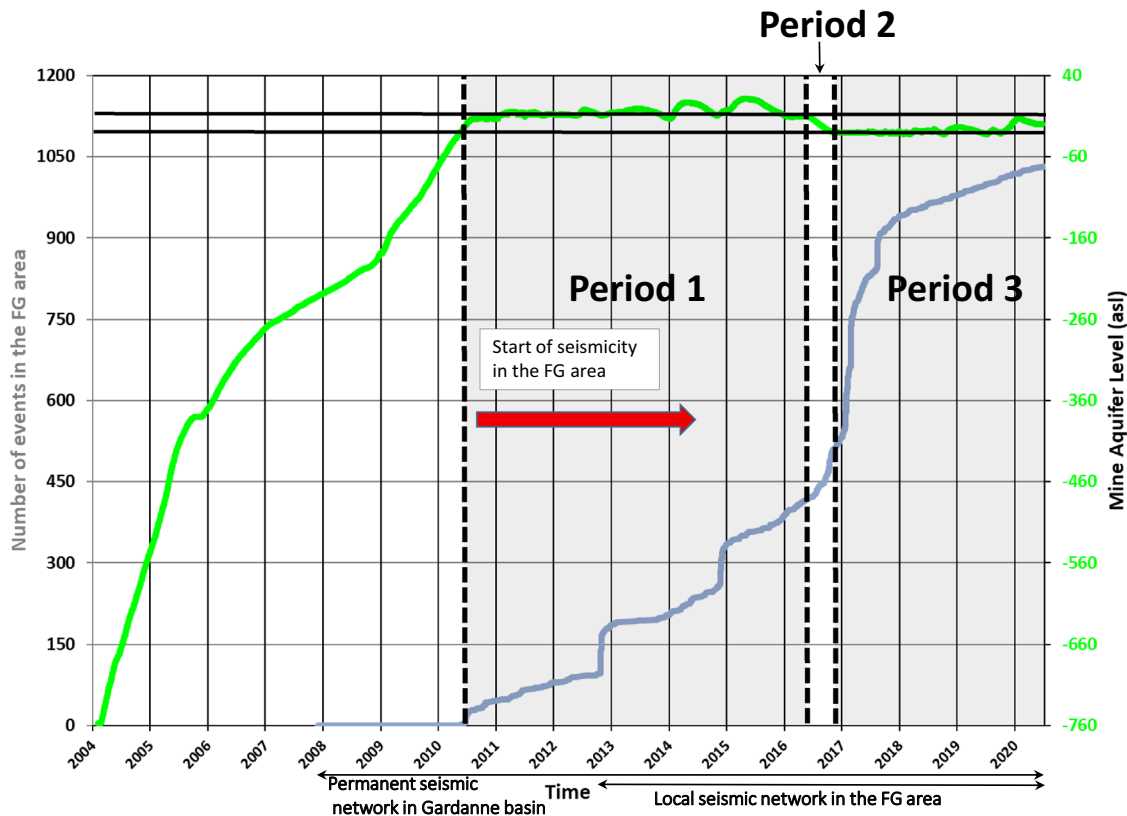


**Fig. 7** Rise of the mine water table recorded at the Gerard shaft (orange dot in Fig. 4) after the 2003 mine closure of Gardanne with the three periods of evolution after 2010. Mine aquifer level at the Gerard shaft (green) and cumulative number of seismic events in the FG area (blue) recorded by the Gardanne permanent seismic network

since the end of 2007. The three periods (dashed lines) are linked to fluctuations in the mine water table. The levels differentiating the periods are marked by two black horizontal lines at  $-10$  m ASL and  $-30$  m ASL

triggered by water table oscillations, particularly after rainy episodes. This seismic background noise extended over a few square kilometers and mostly below the former mine workings; and

- The other, which was more concentrated, occurred in swarms, often with higher magnitudes at the start of the swarm. The rainfall peaks again strongly affected the triggering of the very local microseismic swarms in the FG area. These swarms are most likely linked to the activity of faults crossing mine voids. This triggering occurred  $\approx$  10 days after the effective rainfall peak (and especially sharp rise of the mine water level) during the swarms in November 2012 and December 2014. While the rainfall peaks did not trigger a microseismic swarm, these swarms were systematically preceded by intense rainy episodes sharply raising the level of the mine water table.

The December 2014 swarm was imaged as a clear cloud with a NW–SE trend and a dip towards the NE of  $60^\circ$  (Fig. 8a). This dipping direction does not correspond to the focal mechanism of the 2014/12/01 Mw1.76 event (Table 3 and Fig. 8a), which seems to have a complex source mechanism, as explained above.

Figure 8c also shows the lateral extension to the northwest and southeast of the seismic zone in 2015 compared with that of the seismic swarm in December 2014 (Fig. 8b). This lateral extension is highlighted by the very shallow (less than 300 m) seismic events (in orange in Fig. 8c) towards the south-eastern part during April 2015 when the mine water table was at its highest level (+11 m ASL). This observation seems to correlate perfectly with a rise in the water table to levels never seen before. These events were mainly above the mine workings, which are intersected by the seismogenic zone. At this location, the mine workings are approximately 300 m deep (+20 m ASL). This indicates that these seismic events were mostly above the mine workings and could have affected them. We also observed a very slight trend in the seismicity deepening towards the northwest in parallel with the mine workings.

The estimate of the magnitude considering activation of the entire active surface in 2015—in the event of rupture of the entire seismogenic area—can be made by making the following assumptions (Fig. 8c). Geometrically, we can consider a fault width of 500 m and a fault length of 1400 m for an equivalent source radius of 440 m. A stress drop value  $\Delta\sigma$  of 1 MPa can be considered acceptable in relation to the type of movement for these low magnitude and shallow depth events, which seem to be factors favourable to low values of stress drop (Hough 2014, 2015; Pacor et al. 2016). Using a simple model (Brune 1970), we obtained a moment magnitude (Mw) close to 3.5.

Detailed analysis of sparse seismicity makes it possible to identify concentrations or alignments of events, highlighting new segments that could potentially play a role in the swarms. There are thus three parallel zones trending NW–SE and another smaller swarm trending WNW–ESE to the south (Fig. 9). The microseismicity seems to follow the orientation of known or supposed tectonic faults in the area. This agrees with the identified clusters obtained by automatic location by Namjesnik et al. (2021).

### Second and Third Periods (mid-2016 to the end of 2017)

The second and third periods from mid-2016 to end-August 2017 were marked by frequently repeated seismic swarms stronger in number and energy than those recorded since 2014 (Figs. 5 and 7, supplemental S-1). Nine swarms appeared during these periods compared with two swarms during the first period. The effective rainfall peak and especially sharp acceleration of the rise of the mine water level can explain the first period triggering. This is not the case for these two periods. Therefore, another mechanism for triggering seismicity is proposed.

The beginning of the second period was defined by the dewatering of the flooded mine workings after six years (Fig. 7). Thus, this suggests that over six years, hydrostatic (and seismic) stability was linked to the loading of a water column oscillating between 20 and 40 m (–10 m to +10 m ASL) above the –30 m ASL. Since mid-2016, the dewatering and depressurization caused by a decrease of 20 m of this mine water level (at –30 m ASL) broke a certain hydrostatic equilibrium (green curve in Fig. 10b). It should be noted that this level of the mine aquifer of –30 m ASL corresponds to the first local seismicity in the FG area in 2011.

Since December 2016, the mine water level has been relatively stable at –30 m ASL. Seismic activity increased progressively until March 2017 and then decreased slightly. The last peak of activity began in August 2017, showing a response time of up to  $\approx$  8 months in reaction to the modification of the state of stress. Since the end of 2017, the mine water table has not experienced significant fluctuations, and seismic activity has remained moderate, with about a dozen events per month.

### Seismicity Migration with Mine Water Level

We attempted to statistically correlate the spatial migration of seismicity to the water table evolution of the mine aquifer. For this purpose, the FG area is divided into ten bands 280 m wide (200 m latitude and 200 m longitude) oriented in a NE–SW direction (Fig. 10a).

For each band, the monthly number of seismic events was counted from October 2013 to December 2017. The horizontal histograms in Fig. 10b represent the normalized

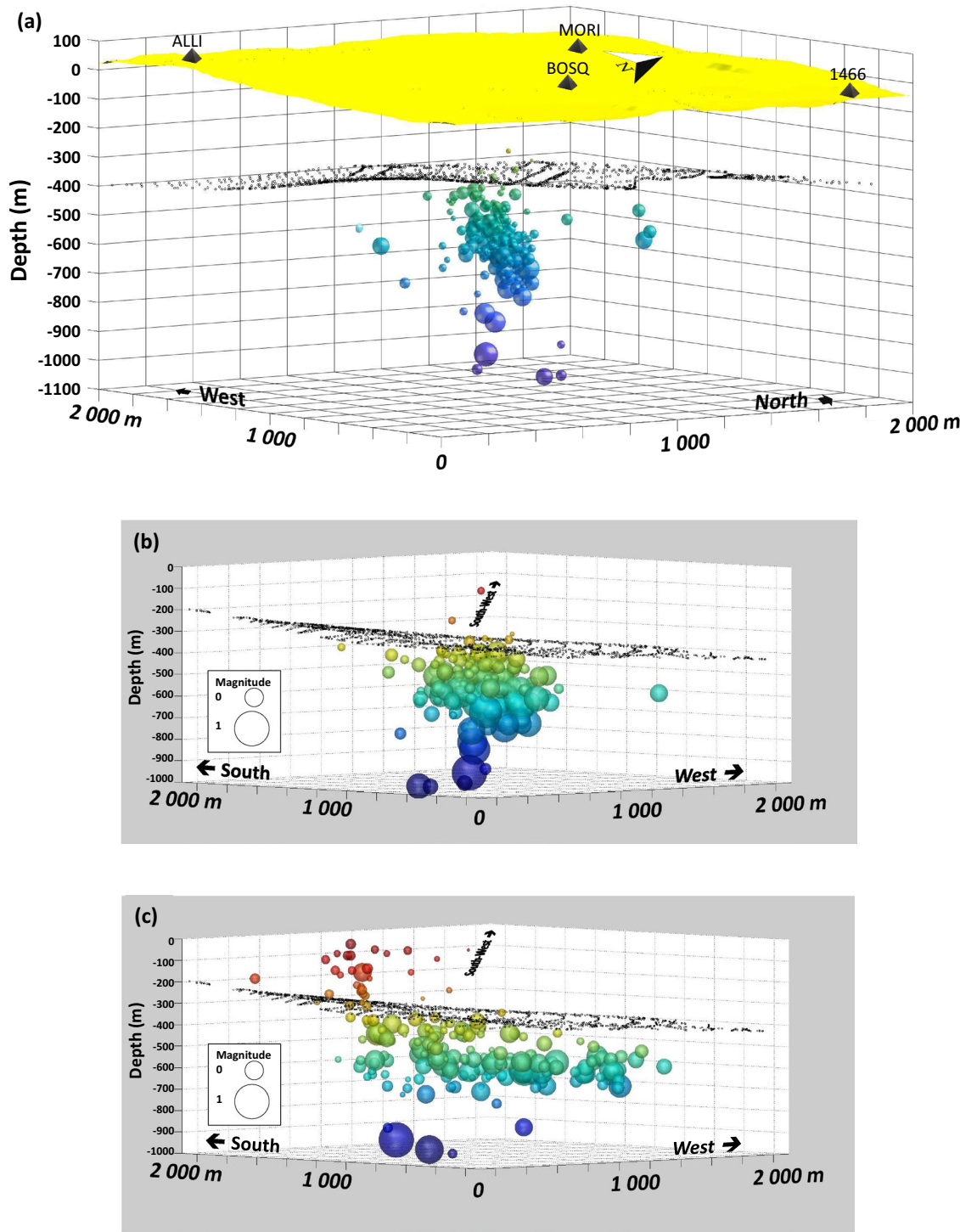


**Fig. 8** **a** 3D distribution of seismic events in the December 2014 swarm. View from the southeast looking to the northwest perpendicular to the fault plane. The size is proportional to the magnitude (from M -1.3 to M 1.4). The colour corresponds to the depth. In black is the mine workings. In yellow is the surface digital elevation model (DEM) in metres (0 corresponds to +330 m ASL). The four seismic stations that recorded the seismic swarms are positioned on the surface DEM. **b** 3D distribution of seismic events in the December

2014 swarm. View from the northeast looking to the southwest. **c** 3D distribution of seismic events in 2015. View from the northeast looking to the southwest. Note the lateral extension of the seismic zone in 2015 compared with that in December 2014, the very shallow seismic events during April 2015 when the mine water table was at its highest level (+11 m ASL) and the very slight trend for the seismicity deepening towards the northwest in parallel with the mine workings

proportion of monthly events in each of the ten bands. For each month, the colour of the band (or geographic portion) varies according to the number of seismic events. The red bar corresponds to the band having the greatest number of seismic events. The black bars correspond to the bands having a median number of seismic events. The grey bars correspond to the bands containing the fewest seismic events. The months whose histograms are completely grey correspond to a monthly seismicity less than or equal to 10 events in the entire FG area (extent of the 10 bands). We consider this low monthly seismicity to be “seismic background noise”, and not representative of the analysis. In other words, the brown curve giving the number of seismic events per month in the FG area indicates the representativeness of the data provided in the histograms. If the number of events is less than or equal to 10, the histogram is not very representative. If the number of events is large (e.g. > 50 events during a seismic swarm), the histogram can be considered very representative for seismicity analysis.

We found a good correlation between the level of the mine aquifer measured at the Gerard shaft (green curve) and the maximum monthly number of seismic events by band area (red bar of the histograms). Fig. 10b clearly shows that over the 2013 to 2017 period, the seismicity was spatially well correlated with the mine aquifer. The low dip of the mine workings (3 to 7° to the northwest) facilitates the lateral drainage of water and the horizontal migration of seismicity. We observe the migration of seismicity to the southeast when the level rises and to the northwest when the level falls. It is interesting to note that this migration is almost synchronous – at the monthly time scale – with the observed water levels. There is probably a slight delay of a few days because the water level measurement is at the Gerard shaft, 6 km west of the FG area (Fig. 4). However, the karstic environment in the FG area greatly facilitates the circulation of water and could explain the small time lag between variations in the water level and the generated seismicity. This rapid circulation was also confirmed by

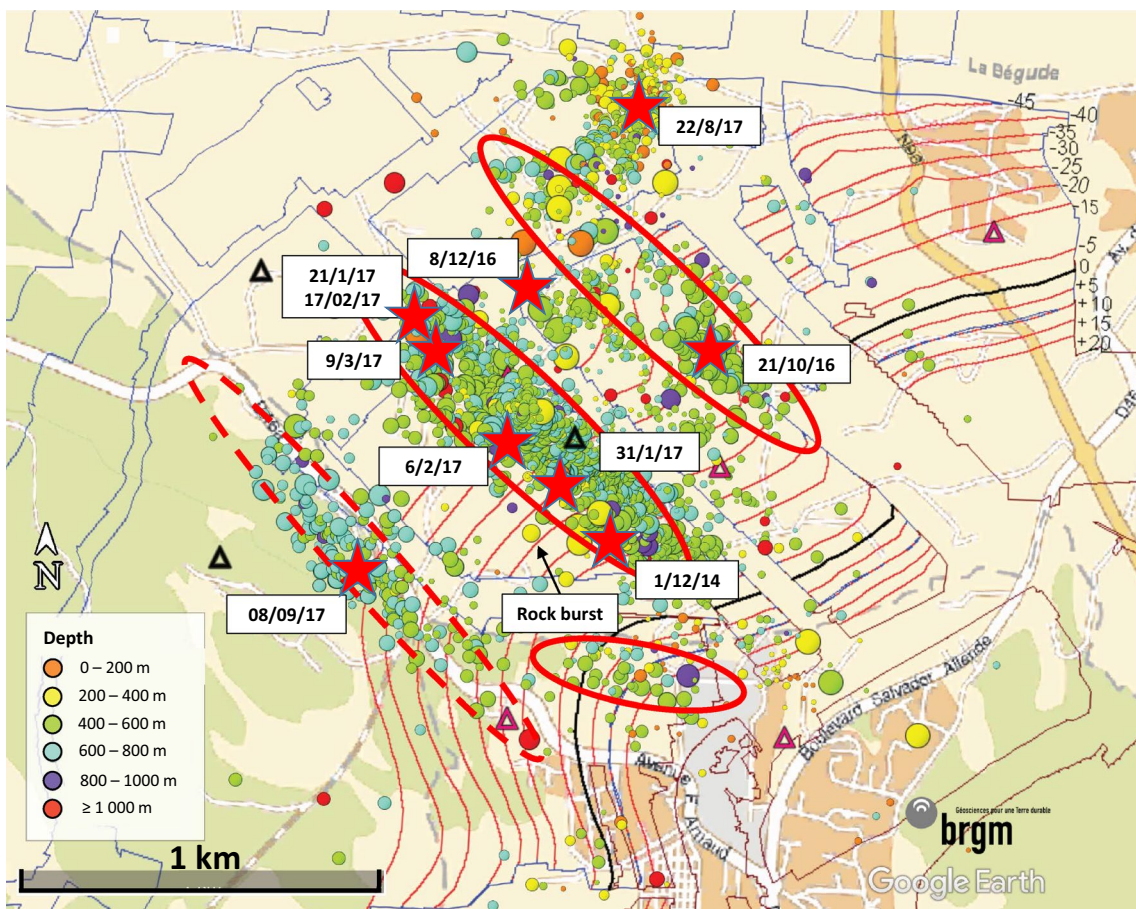


**Fig. 9** Seismicity 2013–2017 in the FG area. In the background, the chamber-and-pillar type mine workings. The lines represent ASL. The seismicity is developed mainly along NE–SW structures parallel to the main trend of the mine workings. Large red stars symbol-

ize seismic swarms. Red ellipses represent the alignments of epicentres to be connected to supposed faults. Focal depth here is measured from the ground surface level (+330 m ASL on average). The rock burst is the isolated yellow dot

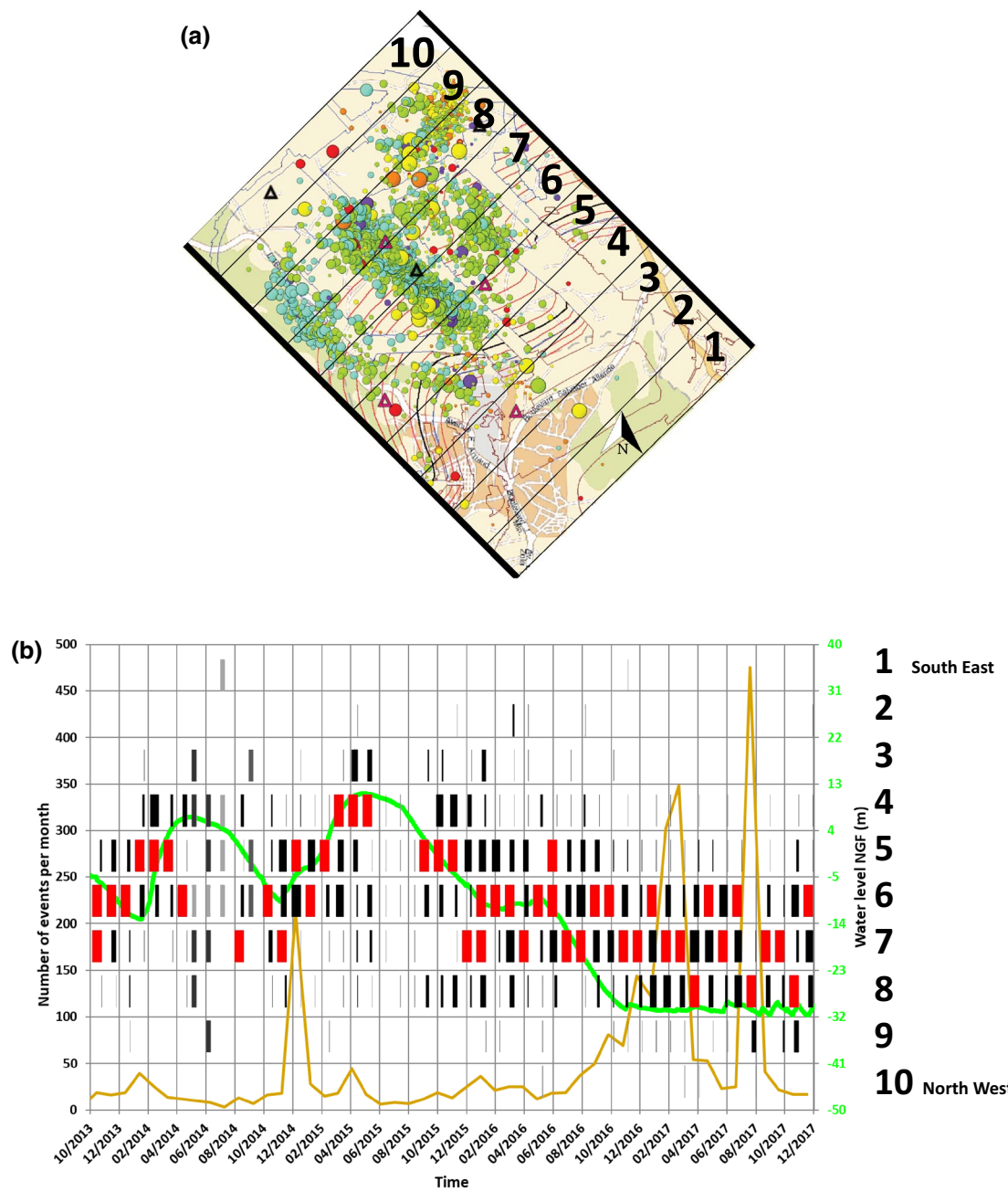


**Fig. 10** **a** Ten geographical bands with their number where the monthly seismicity is counted from October 2013 to December 2017 in the FG area. In the background, the chamber-and-pillar type mine workings and seismicity from October 2013 to December 2017. The lines represent ASL. **b** Mine aquifer level at the Gerard shaft (green curve) and monthly seismicity in the entire FG area (brown curve). The horizontal monthly histograms represent the proportion of seismic events normalized in each band. The red bar shows the band

containing the greatest number of monthly seismic events. The black bar shows the band containing a median number of monthly seismic events. In grey, the histograms for which the monthly number of seismic events is the lowest number of monthly seismic events and considered not to be representative (i.e., less than or equal to 10 seismic events in the FG area). The bold number on the right side of the figure is the band number

the delay - relatively short - of  $\approx 10$  days between effective rains arriving in the basin and the development of seismicity in the FG area (Dominique 2016), as also observed in

other contexts (Bollinger et al. 2010; Dominique et al. 2012; Hainzl et al. 2006; Kraft et al. 2006; Rigo et al. 2008).

One hypothesis related to this migration could be the arrival of water, which would locally modify the velocity

model sufficiently to influence the location of the seismic events and create apparent migration. We did not truly consider this because the "water" interface in the mine voids (= galleries) is too thin (1 to 2 m) to play a role in seismic wave propagation. The waves propagate mostly vertically. For comparison, the wavelength of the P waves remains at a few hundred meters. Thus, such a fluctuation in the structure is always possible, but this does not influence the location analysis, especially if one considers other sources of error (e.g. picking of arrival times and velocity model). For focal mechanism analysis, we use lower frequencies and uncertainty in location is less important.

We can estimate that for a water height variation of 1 m in the mine aquifer, the seismicity migrates on the order of 20 to 40 m towards the SE (if the water level increases) or towards the NW (if the water level decreases). Of course, this estimate is only a trend and does not prevent the development of sparser seismicity.

We also observe that all seismic swarms after the end of 2016 (water level at  $\approx -30$  m ASL) are found further northwest than those in December 2014 (water level at  $\approx -5$  m ASL), that is, in bands with a number greater than 5. Likewise, the last major swarm in August 2017 was the most northwestern swarm (band 8) (Figs. 9 and 10b).

### The Case of Pillar or Roof Fall/Rock Burst

From the beginning of significant seismicity in the FG area with the seismic swarm in November 2012, collapses of the roof of the galleries or pillar bursts were suspected. This is one of the main reasons why the local temporary seismic network was deployed in the FG area. However, the frequency, nature, epicentre location, and focal depth of the seismic events were not compatible with such a phenomenon. Finally, out of thousands of seismic events analysed, only the event on February 1, 2017, 4h45 UT, shows the characteristics of an underground mining seismic event (blast or roof collapse; asterisk in Table 4).

Several arguments support this hypothesis of a mining event. First, the shape of the signal can be easily differentiated from the events that occurred just before. Two events

of equivalent magnitude at 1.5 and 1.2 s earlier (Table 4 and Supplemental Fig. S-3a) are compared. The gradual monochromatic rise "in the funnel" of the wave differs from that observed just before, representative of an earthquake. The Fourier spectrum shows large differences between both types of waves. The spectrum of the mining event shows a higher frequency content (between 65 and 80 Hz) (Supplemental Fig. S-3c) than that of natural seismic events (between 15 and 30 Hz) (Supplemental Fig. S-3b).

Then, this event occurred after a series of three seismically felt events: on January 18, January 31, and February 1. The swarm of January 31—February 2 generated 38 events on January 31. The strongest event on January 31 at 2h54 UT had the greatest acceleration (nearly  $70 \text{ cm/s}^2$ ) recorded on a sensor (ROSS station) since installation of the local network, producing the maximum moment magnitude of Mw 1.94 of the catalogue (Table 3). It also occurred just 1 s after two nearby significant events of  $\approx$  magnitude 1. We can therefore assume that a series of these significant events may have destabilized the roof of the galleries or certain pillars, causing their collapse. We also note that the depth of this event was more superficial than most of the seismicity in the sector. Finally, it was isolated without any direct association with swarms already identified in this area (e.g. Figure 9 and supplemental Fig. S-4). All these elements suggest that a local destabilization of mine workings occurred on Feb. 1, 2017.

### Conclusion

This paper explores the seismicity triggered by the rise and oscillations of the water table in former mine workings in Gardanne, southern France, after mine closure in 2003. We focused on the period between 2013 and 2017 using a new seismic network installed after the seismic swarm of December 2012.

Our observations showed that triggered seismicity closely depends on the period and amplitude of mine water table variations. The low dip of the mine workings used as a privileged drain favoured a seismic migration in a NW–SE

**Table 4** Parameter characteristics of the main seismic events in January and early February 2017. The event marked by an asterisk is suggested as a mining event. The seismograms of 01/02 16h45 are shown in Fig. 13. The map of seismic events is shown in Fig. 14

| Date                     | 18/01              | 31/01              | 01/02 16h45        |                    |                    | 01/02              | 02/02              |
|--------------------------|--------------------|--------------------|--------------------|--------------------|--------------------|--------------------|--------------------|
|                          | Hour, Minute       | 23h02              | 02h54              |                    |                    | 16h48              | 05h01              |
| Second (TU)              | 5.3 s              | 28.1 s             | 33.9 s             | 34.2 s             | 35.4 s (*)         | 49.3 s             | 23.9 s             |
| Latitude<br>(° decimal)  | 43.441°N<br>± 50 m | 43.443°N<br>± 50 m | 43.444°N<br>± 50 m | 43.444°N<br>± 50 m | 43.442°N<br>± 50 m | 43.444°N<br>± 75 m | 43.444°N<br>± 50 m |
| Longitude<br>(° decimal) | 5.539°E<br>± 50 m  | 5.534°E<br>± 50 m  | 5.534°E<br>± 50 m  | 5.534°E<br>± 50 m  | 5.533°E<br>± 50 m  | 5.533°E<br>± 75 m  | 5.525°E<br>± 50 m  |
| Depth (m)                | 500<br>± 50        | 640<br>± 50        | 640<br>± 50        | 640<br>± 50        | 240<br>± 150       | 860<br>± 75        | 610<br>± 50        |
| Local Magnitude          | 1.4                | 1.6                | 1.1                | 1.1                | 0.8                | 1.6                | 1.2                |

direction according to the water table oscillations. Most seismicity was found below the mine workings between 400 and 800 m below the ground surface (100 to 500 m below the mine workings). In addition, it was observed that the shallowest events ( $\approx 200$  m) occurred above the mine workings and in the southeastern part of the FG area (Fig. 8). This also seems consistent with a rise in mining levels towards the southeast.

The focal mechanisms achieved in this study, the northeastern dip of the main faults, the NW–SE direction of the events of the 2014 swarm, and the extension regime described by several authors in the FG area (Chalumeau 2000; Gaviglio 1987; Gaviglio et al. 1996) agree with normal faults in a NW–SE direction (Figs. 2, 6, and 9). The two main clusters in the NW–SE direction are on the eastern part of the exploited mine workings. The upward extension of the fault surface crossing the mine workings at a depth of  $\approx 300$  m ( $\approx 0$  m ASL) arrives in the middle of the exploited panels, which can be considered as reservoirs. This configuration would correspond to the destabilization scheme proposed by Talwani (1997), taking up an analysis by Roeloffs (1988).

As described by other authors for reservoir-induced seismicity (RIS), this seismicity can be qualified as continuously triggered seismicity or protracted seismicity (Talwani 1997) due to its persistence over time. In addition to the highly activated seismic periods, nearly ten events are still recorded every month. This implies that this seismicity will exist as long as the water level remains and fluctuates above – 30 m ASL. A clear migration of seismicity with the oscillations of the mine aquifer depending on the pumping capacities and effective rains is highlighted. The seismically activated area corresponds to a fault size of Mw3.5 earthquake. All these points lead to the necessity of continuous hydraulic and seismic monitoring to better understand these phenomena and to assess the related risks.

**Supplementary Information** The online version contains supplementary material available at <https://doi.org/10.1007/s10230-022-00860-z>.

**Acknowledgements** The authors thank the French Ministry for the Ecological and Inclusive Transition, for financial support. This work is a contribution to the Research Fund for Coal and Steel (RFCS 2019) by the European Commission—Directorate-General for Research and Innovation under the Grant agreement (899192)—PostMinQuake. All the reservoir data were provided by the BRGM—Department for Mine Safety and Risk Prevention (DPSM). The seismic data are coming from BRGM. Additional seismic data are furnished by Ineris. The BRGM seismic catalogue is freely downloadable at through the BRGM [https://doi.org/10.18144/0\\_f4f64ebf-b3b5-4462-b374-61955a40a0fe](https://doi.org/10.18144/0_f4f64ebf-b3b5-4462-b374-61955a40a0fe). We used MATLAB ver R2018a for some figures and the Software SeisGram2K Seismogram Viewer v7.0.0X10 (29Mar2016) (BETA)—Copyright (C) 2000–2016 Anthony Lomax ([www.alomax.net](http://www.alomax.net)) for data viewing and processing. Finally, we are very grateful to the three anonymous reviewers whose comments greatly improved the quality of the manuscript.

**Open Access** This article is licensed under a Creative Commons Attribution 4.0 International License, which permits use, sharing, adaptation, distribution and reproduction in any medium or format, as long as you give appropriate credit to the original author(s) and the source, provide a link to the Creative Commons licence, and indicate if changes were made. The images or other third party material in this article are included in the article's Creative Commons licence, unless indicated otherwise in a credit line to the material. If material is not included in the article's Creative Commons licence and your intended use is not permitted by statutory regulation or exceeds the permitted use, you will need to obtain permission directly from the copyright holder. To view a copy of this licence, visit <http://creativecommons.org/licenses/by/4.0/>.

## References

Aochi H, Burnol A (2018) Mechanism of the ML4.0 25th April 2016 earthquake in southwest of France in the vicinity of the Lacq gas field. *J Seismol* 22:1139–1155. <https://doi.org/10.1007/s10950-018-9758-5>

Baroux E, Bethoux N, Bellier O (2001) Analyses of the stress field in southeastern France from earthquake focal mechanisms. *Geophys J Int* 145:336–348. <https://doi.org/10.1046/j.1365-246x.2001.01362.x>

Baroux E, Pino NA, Valensise G, Scotti O, Cushing M (2003) Source parameters of the 11 June 1909, Lambesc (southern France) earthquake: a reappraisal based on macroseismic, seismological and geodetic observations. *J Geophys Res* 108(B9):2454. <https://doi.org/10.1029/2002JB002348>

Bertil D, Cansi Y, Descloires M, Hyvernaud O, Massinon B, Plantet JL, Santoire JP (1987) Study of the seismicity of the Gardanne basin, French Alternative Energies and Atomic Energy Commission Report [in French]

Bollinger L, Nicolas M, Marin S (2010) Hydrological triggering of the seismicity around a salt diapir in Castellane. France, *Earth Planet Sci Lett* 290:20–29. <https://doi.org/10.1016/j.epsl.2009.11.051>

Bour M, Foussac D, Dominique P, Martin C (1998) On the use of microtremor recordings in seismic microzonation. *Soil Dyn and Earthquake Eng* 17:465–474. [https://doi.org/10.1016/S0267-7261\(98\)00014-1](https://doi.org/10.1016/S0267-7261(98)00014-1)

Brune JN (1970) Tectonic stress and the spectra of seismic shear waves from earthquakes, *J Geophys Res* 75:4997–5009. <https://doi.org/10.1029/JB075i026p04997>

Cara M, Cansi Y, Schlupp A et al (2015) SI-Hex: a new catalogue of instrumental seismicity for metropolitan France. *Bull Soc Géol Fr* 186(1):3–19. <https://doi.org/10.2113/qssqfbull.186.1.3>

Calais E, Nocquet JM, Jouanne F, Tardy M (2002) Current strain regime in the Western Alps from continuous global positioning system measurements, 1996–2001. *Geology* 30(7):651–654. [https://doi.org/10.1130/0091-7613\(2002\)030%3c0651:CSRITW%3e2.0.CO;2](https://doi.org/10.1130/0091-7613(2002)030%3c0651:CSRITW%3e2.0.CO;2)

Chalumeau A (2000) Hydrogeological functioning of lignite operations in the Fuveau basin (Bouches-du-Rhône). PhD Diss, UFR des Sci et Techn Univ Franche-Comté—798 [in French]

Delacou B, Sue C, Champagnac JD, Burkhard M (2004) Present-day geodynamics in the bend of the western and central Alps as constrained by earthquake analysis. *Geophys J Int* 158(2):753–774. <https://doi.org/10.1111/j.1365-246X.2004.02320.x>

Devoti R, D'Agostino N, Serpelloni E, Pietrantonio G, Riguzzi F, Avalone A et al (2017) A combined velocity field of the Mediterranean region. *Ann Geophys* 60(2):S0215. <https://doi.org/10.4401/ag-7059>

Dewandel B, Ladouche B, Lanini S (2017) Research project ARK. Improved knowledge of the aquifer in the Aix-Gardanne basin.

BRGM Report BRGM/RP-65884-FR, <http://infoterre.brgm.fr/rapports/RP-65884-FR.pdf> Accessed 2021–11–29 [in French]

Didier Ch, Laouafa F, Thoraval A, Tritsch J-J (2003) Coal basin of Provence. Study of the effects on surface terrains of underground mining works and their foreseeable evolution over time. Vol. 1, 2, & 3, INERIS Report DRS-03–364607R01 [in French]

Dheilly A, Brigati B (2015) Management of the Gardanne mining reservoir, Bouches du Rhône: Environmental and hydraulic approaches to pumping and its discharge into the Mediterranean Sea. Past and present mining operations: environmental and societal impacts, pp 71–84, Coll. EDYTEM. HAL Id: hal-01100951. <https://hal-brgm.archives-ouvertes.fr/hal-01100951> [in French]

Dominique P, Le Loher F, Bendif M (2012) Instrumentation of a small seismic crisis in Salsigne (Aude), JNGG, Bordeaux. 934 p., 2 vol., 91–98. <https://hal-brgm.archives-ouvertes.fr/hal-00822447/document> Accessed 2021–11–29 [in French]

Dominique P (2016) Microseismicity in a mining context-The Gardanne coal basin (Bouches-du-Rhône), 1280–1287. [https://jngg2016.sciencesconf.org/80835/JNGG\\_Nancy\\_2016\\_micr0sismicite\\_Gard.pdf](https://jngg2016.sciencesconf.org/80835/JNGG_Nancy_2016_micr0sismicite_Gard.pdf) Accessed 2021–11–29 [in French]

Dünner C (2011) 2010 annual monitoring report for areas overlying mining buildings at risk of sinking of a brittle nature - coal basin of Provence. Study Report DRS-11–120558–03174A [in French]

Gaviglio P (1987) Consequences of structural change on the physical characteristics of fuvelian limestones in the Arc Basin (Bouches-du-Rhône, France): fracturing, mechanical properties, stress states. *Geol Mediterr* 14(3):221–232. [https://doi.org/10.3406/geolm.1987.1384\[inFrench\]](https://doi.org/10.3406/geolm.1987.1384[inFrench])

Gaviglio P, Bigarre P, Baroudi H, Piguet J-P, Monteau R (1996) Measurements of natural stresses in a Provence mine (Southern France). *Eng Geol* 44:77–92. [https://doi.org/10.1016/S0013-7952\(96\)00041-5](https://doi.org/10.1016/S0013-7952(96)00041-5)

Goldbach O (2010) What is the seismic risk of mine flooding? CSIR, Pretoria. <http://hdl.handle.net/10204/4256> Accessed 2022–01–12

Goldberg D (1989) Genetic Algorithms in Search, Optimization, and Machine Learning, Addison-Wesley Professional, ISBN 978-0201157673

Gonzalez G (1990) Public information project on the Gardanne mining basin (Bouches-du-Rhône). Natural site conditions. File no. 1: The Deposit: Nature, Geometry, Quality. BRGM Report BRGM/R 30960 PAC 4S 90 <http://infoterre.brgm.fr/rapports/RR-30960-FR.pdf> Accessed 2021–11–29 [in French]

Haessler H, Hoang-Trong P, Legros Y (1985) The seismic event of February 19, 1984 in western Provence: tectonic earthquake or mining blow? P. Melchior (ed.), Seismic Activity in Western Europe, 223–232. D. Part of the NATO ASI Series book series (ASIC, 144). Reidel Publ. Comp. [https://doi.org/10.1007/978-94-009-5273-7\\_18](https://doi.org/10.1007/978-94-009-5273-7_18) [in French]

Hainzl S, Kraft T, Wassermann J, Igel H, Schmedes E (2006) Evidence for rainfall-triggered earthquake activity. *Geophys Res Lett* 33:L19303. <https://doi.org/10.1029/2006GL027642>

Hough SE (2014) Shaking from injection-induced earthquakes in the central and eastern United States. *Bull Seismol Soc Am* 104(5):2619–2633. <https://doi.org/10.1785/0120140099>

Hough SE (2015) Shaking intensity from injection-induced versus tectonic earthquakes in the central-eastern United States. *Lead Edge* 34(6):690–697. <https://doi.org/10.1190/tle34060690.1>

Jomard H, Scotti O, Auclair S, Dominique P, Manchuel K, Sicilia D (2021) - The SISFRANCE database of historical seismicity. State of the art and perspectives. C R - Geosci as part of the BCSF centenary. ISSN (electronic): 1778–7025. <https://doi.org/10.5802/crgeos.91>. Online first, 8 Dec. 2021

Kraft T, Wassermann J, Schmedes E, Igel H (2006) Meteorological triggering of earthquake swarms at Mt Hochstaufen. SE-Germany, Tectonophysics 424:245–258. <https://doi.org/10.1016/j.tecto.2006.03.044>

Lee WHK, Lahr JC (1975) Hypo71 (revised): a computer program for determining hypocenter, magnitude, and first motion of local earthquakes. Open-file report 75–311, <https://pubs.usgs.gov/of/1975/0311/report.pdf>.

Manchuel K, Traversa P, Baumont D, Cara M, Neyman E, Durouchoux C (2018) The French seismic CATalogue (FCAT-17). *Bull Earthq Eng* 16:2227–2251. <https://doi.org/10.1007/s10518-017-0236-1>

MATLAB (2017) Release 2017.a, version 9.2.0.556344.1 Natick, Massachusetts: The MathWorks, Inc.

Moulin M (2010) Hydrogeological study of deep groundwater resources in the Aix - Gardanne basin. Report BRGM/RP-57641-FR. <http://infoterre.brgm.fr/rapports/RP-57641-FR.pdf> Accessed 2021–11–29 [in French]

Nakamura Y (1989) A method for dynamic characteristics estimation of subsurface using microtremor on the groundsurface. *Rep Railway Tech Res Inst* 30(1):25–33

Namjesnik D, Kinscher J, Gunzburger Y, Poiata N, Dominique P, Bernard P, Contrucci I (2021) Automatic detection and location of microseismic events from sparse network and its application to post-mining monitoring. *Pure Appl Geophys* 178:2969–2997. <https://doi.org/10.1007/s00024-021-02773-4>

Pacor F, Spallarossa D, Oth A, Luzi L, Puglia R, Cantore L, Mercuri A, D'Amico M, Bindi D (2016) Spectral models for ground motion prediction in the L'Aquila region (central Italy): evidence for stress-drop dependence on magnitude and depth, *Geophys J Int* 204(2):697–718. <https://doi.org/10.1093/gji/ggv448>

Rigo A, Béthoux N, Masson F, Ritz J-F (2008) Seismicity rate and wave-velocity variations as consequences of rainfall: the case of the catastrophic storm of September 2002 in the Nîmes Fault region (Gard, France). *Geophys J Int* 173:473–482. <https://doi.org/10.1111/j.1365-246X.2008.03718.x>

Roeloffs EA (1988) Fault stability changes induced beneath a reservoir with cyclic variations in water level. *J Geophys Res* 93:2107–2124. <https://doi.org/10.1029/JB093iB03p02107>

Rouire J, L'Homer A, Blanc J-J (1979) Carte géologique de la France à 1/250 000, feuille de Nice, BRGM Ed. [in French]

Senfaute G, Wassermann J, Homand F (2008) Induced micro-seismicity and mechanical response during the experimental flooding of an iron ore mine. *Symp. Post-Mining ASGA. Vandoeuvre-les-Nancy*, p. 11. <https://hal-ineris.archives-ouvertes.fr/ineris-00973288> Accessed 2022–01–12

SisFrance (2016) BRGM-EDF-IRSN. Sismicité historique de la France métropolitaine. [www.sisfrance.net](http://www.sisfrance.net) Accessed 2021–11–29 [in French]

Talwani P (1997) On the nature of reservoir-induced seismicity. *Pure Appl Geophys* 150:473–492. <https://doi.org/10.1007/s000240050089>

Terrier M, Vermeersch F, Rey J, coll. Rouillé A, Bertrand G (2008) Press file on seismic hazards for 6 French regions. Report BRGM/RP-56448-FR. <http://infoterre.brgm.fr/rapports/RP-56448-FR.pdf> Accessed 2021–11–29 [in French]

Ulrich T, Aochi H (2015) Rapidness and robustness of finite source inversion from elliptical patches method using continuous GPS and acceleration data: 2011 Mw9.0 Tohoku earthquake. *Pure Appl Geophys* 172:3439–3453. <https://doi.org/10.1007/s00024-014-0857-0>

Worden CB, Gerstenberger MC, Rhoades DA, Wald DJ (2012) Probabilistic relationships between ground-motion parameters and modified Mercalli intensity in California. *Bull Seismol Soc Am* 102(1):204–221. <https://doi.org/10.1785/0120110156>